1   # Supporting Information

2   # The influence of electric fields on biofouling of carbonaceous

3   # electrodes

4

5   Soumya Pandit[1], Sneha Shanbhag[2], Meagan Mauter[2,3], Yoram Oren[1] and Moshe

6   Herzberg[1]*

7

8   Author Affiliations:

9   [1] Zuckerberg Institute for Water Research, Blaustein Institutes for Desert Research, Ben

10   Gurion University of the Negev, Midreshet Ben Gurion, 84990, ISRAEL

11   [2] Department of Civil & Environmental Engineering, Carnegie Mellon University, 5000

12   Forbes Ave., Pittsburgh, PA, 15213, USA

13   [3] Department of Engineering and Public Policy, Carnegie Mellon University, 5000

14   Forbes Ave., Pittsburgh, PA, 15213, USA

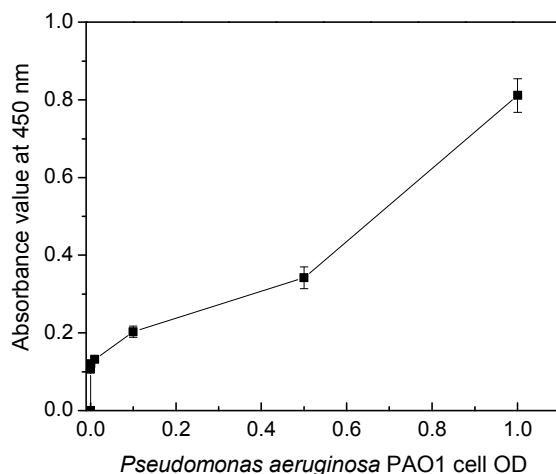15

16   *Author to Whom Correspondence Should Be Addressed

17   E-mail: herzberg@bgu.ac.il

18   Phone: +972-86563520

19

20   Number of pages: S1-S23 (23)

21   Number of figures: S1-S16 (16)

22 **SI-1 Growth curve experiment for wild type *Pseudomonas aeruginosa PAO1* and**

23 **Calibration curve of XTT assay**

24

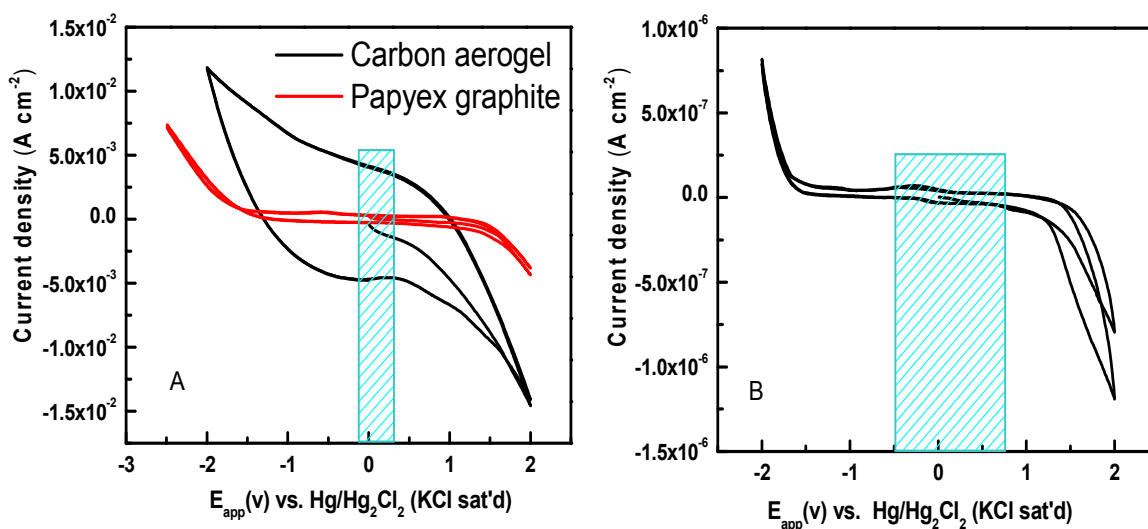25   *Figure S-1: Calibration curve of XTT assay*

26

27 **SI-2 Construction of the customized flow cell**

28   A customized parallel plate electrochemical flow-cell was constructed and the details

29 of preparation steps are explained as follows: (1) The reference electrode terminal was

30 attached to the counter electrode terminal by a crocodile clip; (2) the working electrode

31 terminal was connected to a thin aluminum foil (1.5 μm) via a copper stick; (3) an indium

32 tin oxide (ITO)-covered electrically conductive glass slide was wired to a potentiostat

33 instead of a regular cover-glass using a platinum foil; and (4) the carbon or graphite at the

34 bottom of the flow chamber was used as working electrode. The constant voltage was

35 applied with a potentiostat (Prinston Applied Research), and then the resulting electric

36 current was monitored via the affiliated computer program (ECHEM). The voltage was

37 also recorded by a data-logger (EXTech Instruments). Additionally, the working

38 electrode for biofilm growth study was connected with a thin aluminum foil as a current

39 collector. The conductive side of ITO slide was adjusted to a 0.5 μm thick platinum frame

40 at its edges in order to distribute the electrical potential as much uniformly as possible

41 throughout the entire flow-channel.

42

SI-3 Determination of working and counter electrode's voltage window
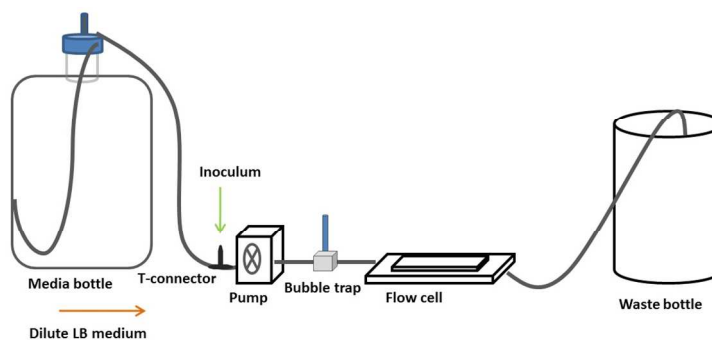
The range of voltages applied to the electrodes (voltage window) is an important parameter in the flow cell experiments. In general, a potential range should be selected where current does not change abruptly with applied potential. In this research, the effective voltage window of the different working and counter electrodes were studied by cyclic voltammetry (CV) using Princeton 273a potentiostat. A three-electrode configuration consisting of PA, CA and ITO coated glass as working electrodes and Pt wire and Hg/Hg_2Cl_2 (KCl sat'd) as counter and reference electrodes, respectively, was used for all the CV measurements using an electrochemical cell (Metrohm Autolab). The solution was the same as used in the flow cell experiments, namely, 10% LB medium supplemented with 0.1 M Na_2SO_4. Cyclic voltammograms (Figures S-2 A and B) were recorded in the potential range of -2.0 V to +2.0 V at a scan rate of 5 mV/s. The initial and final potential was kept constant at 0.1 V (close to OCP).

In the flow cell experiments, different voltages were applied between the counter (ITO) electrode and the working (PA or CA) electrodes at the voltage range +0.9V to -0.9 V. This corresponds to a voltage window of -70mV to +250mV while at the same time that for ITO was between -550mV and +350 mV (all values are vs. Hg/Hg_2Cl_2, KCl sat'd). As depicted in Figures S-2A and S2-B by the dashed bars, these windows are well within the range where Faradic reactions (such as water electrolysis) can be considered insignificant. These ranges correspond to a maximum voltage window of -0.9V to +0.9V between the working (PA or CA) and the counter (ITO) electrodes. As depicted in Figure S-2A by the dashed bar, this window is well within the range were Faradic reactions (such as water electrolysis) can be considered insignificant.

68 ***Figure S-2***: *Cyclic voltammograms at a scan rate of 5 mV/sec using 10% LB medium*
69 *supplemented with 0.1 M Na$_2$SO$_4$ as an electrolyte. A) Working electrodes- Carbon*
70 *aerogel and Papyex graphite. B) ITO coated glass slide. The dashed bar in Figure A*
71 *shows the voltage range, in terms of working electrode vs. reference electrode,*
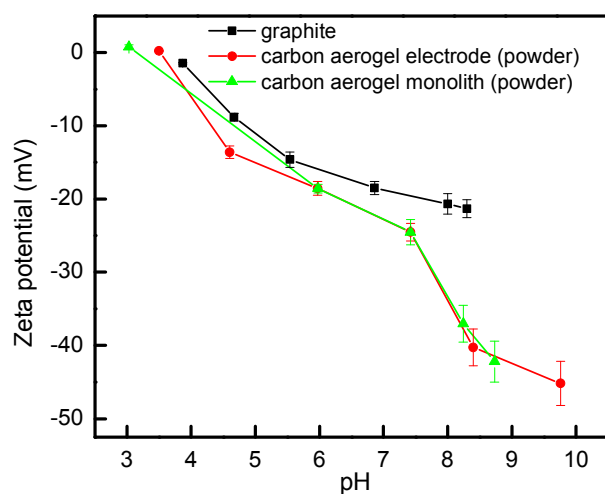72 *corresponding to the voltage range applied in the flow cell experiments.*

73

74

75 **SI-4 Scheme of flow cell set-up**

76

77

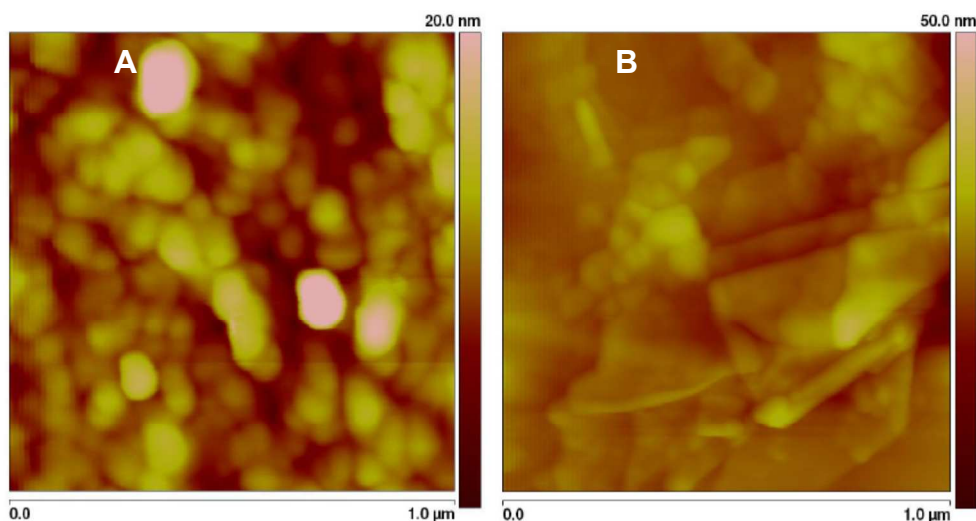78   ***Figure S-3:*** *Schematic of flow cell set-up*

79 **SI-5 Zeta potential measurements for carbon electrodes**

80   As it is shown in Figure S-4, there was not any significant difference between the zeta

81   potentials of monoliths versus electrodes. Accordingly, the results demonstrated that at

82   pH above 7, zeta potentials of graphite and carbon aerogel variants diverge, which could

83   be attributed to the pKa values of different chemical functional groups, such as

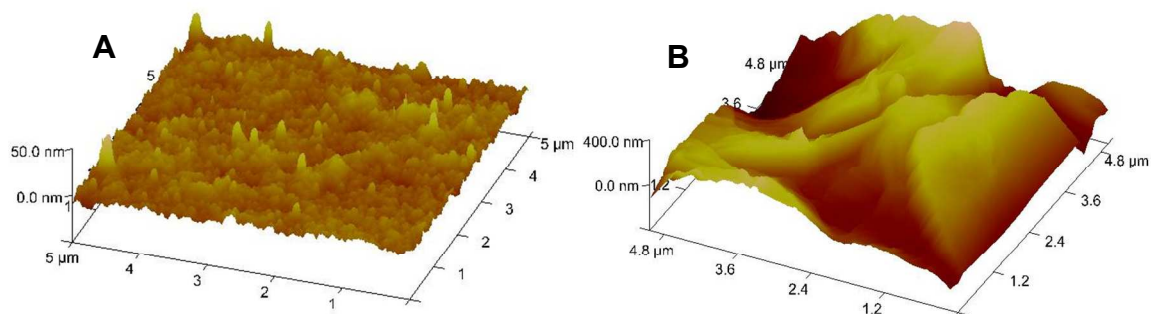84   carboxylic and carbonyl group on two different surfaces.

85

86

87   ***Figure S-4.*** *Zeta potentials of carbon aerogel and graphite vs. pH titrations. All samples*

88   *were measured in an electrolyte of 0.001 M NaCl and titrated with 0.1M HCl or 0.1 M*

89   *NaOH. The error bars represent one standard error of at least eight readings*

90

91

92 **SI-6 Roughness and topography of the carbon surfaces**

93

94 ***Figure S-5:*** *AFM visualization of carbon aerogel, CA (A) and graphite paper, PA (B) at*

95 *a resolution of 1 μm^2. The z-scale is depicted on the right to each frame and covers a*
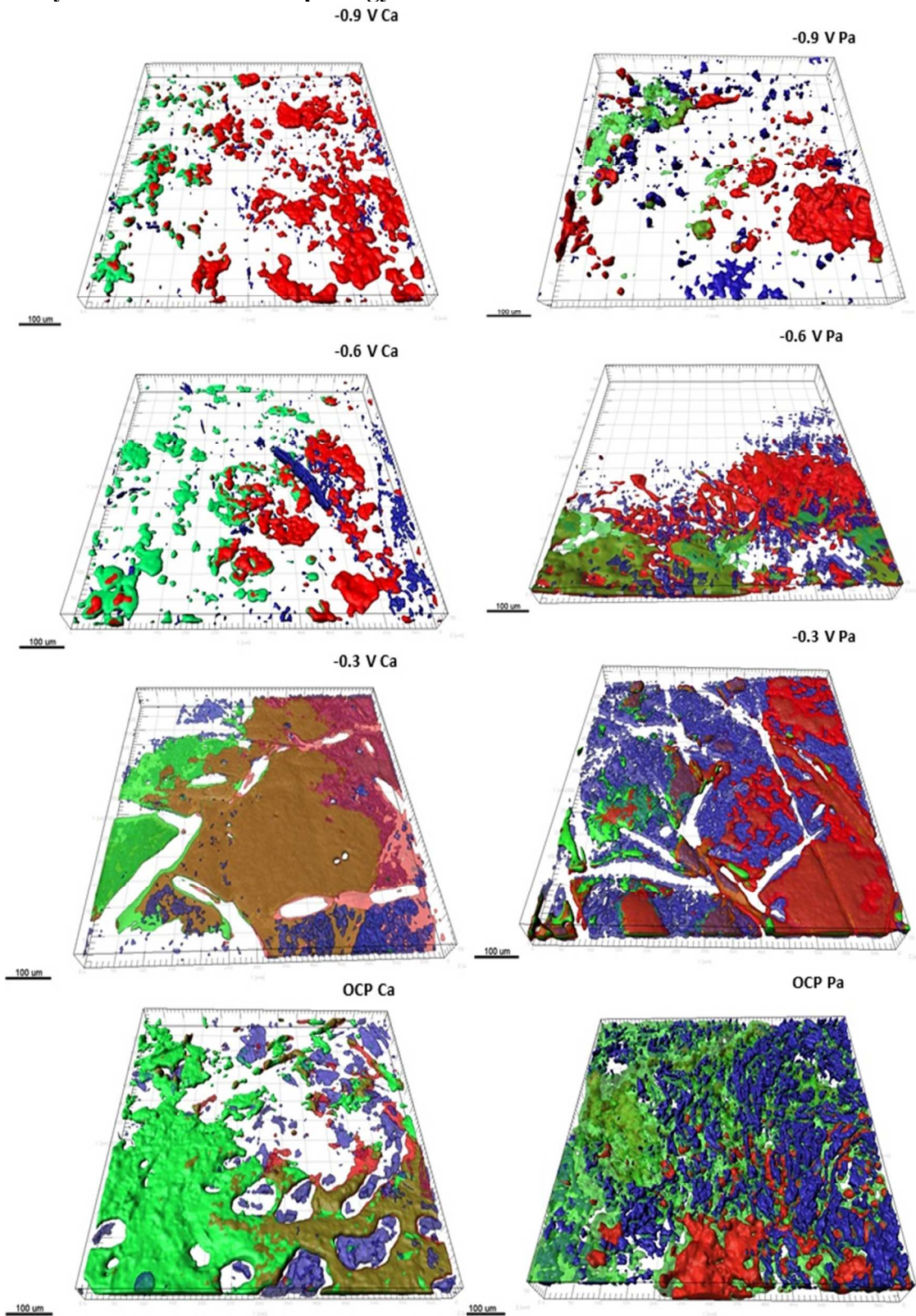
96 *broader range in graphite.*

97 ***Figure S- 6:*** *3D visualization of carbon aerogel, CA- A; and graphite, PA- B: at a*

98 *resolution of 5 μm^2. In graphite, the range of the z-scale is four times the range in carbon*

99 *aerogel.*

100

101 **SI-7 Investigating the interaction between the produced formazan salt dye with**
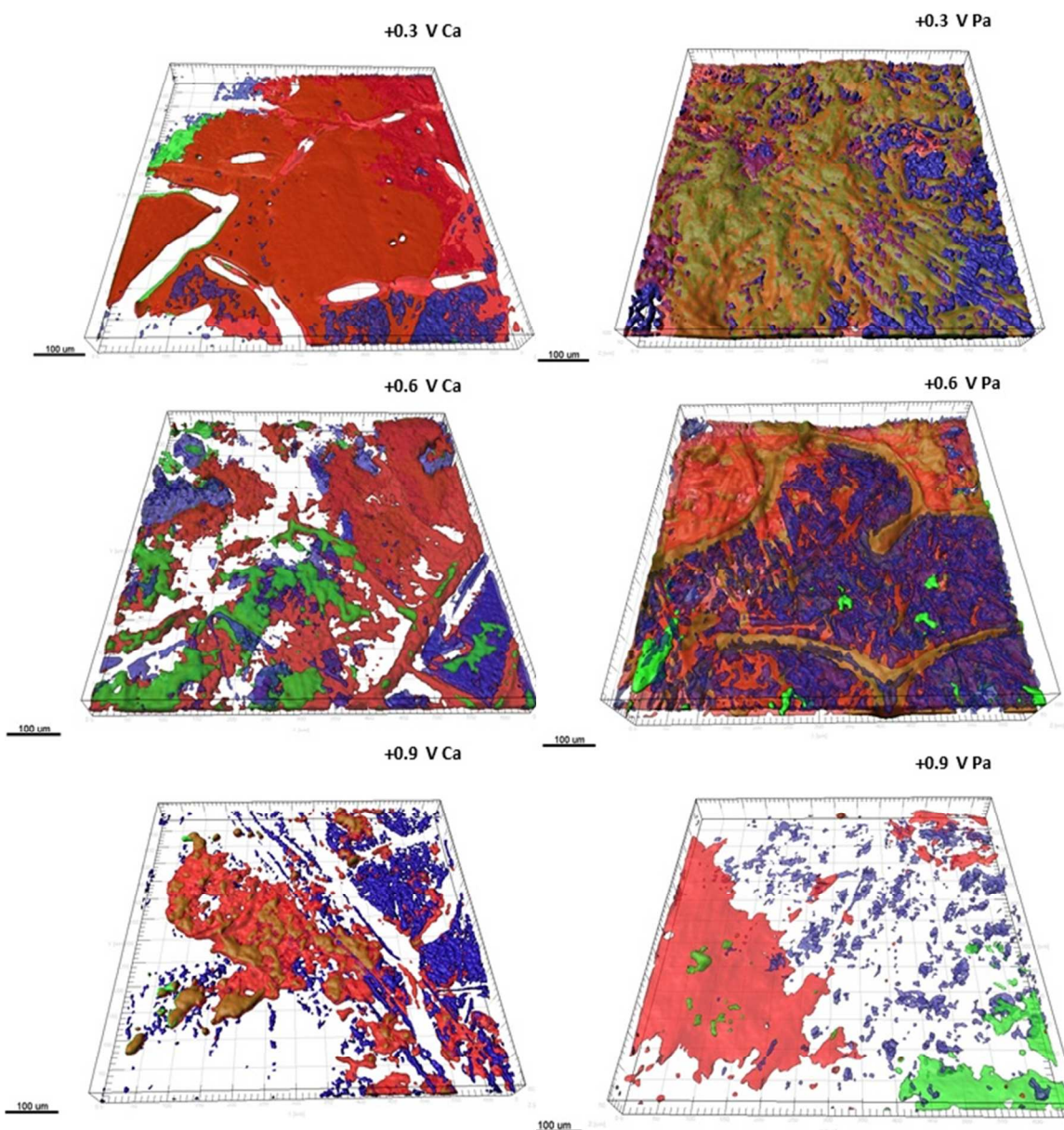
102 **carbon particles**

103   In order to prove the lack of any interaction between the produced formazan salt dye with

104   carbon particles, formazan salt containing solution was collected after 2 h incubation in a

105   multiplate reader instrument with XTT reagent and bacterial suspension. After

106   centrifugation, the supernatant was divided in to halves of 50 µL and 50 µL. Then DDW

107   was added in one Eppendorf tube while 50 µL carbon particles suspended solution was

108   added to the other one. It is worth mentioning that the experiment was done in dark room

109   to avoid photo bleaching. The absorbance measurements were carried out after keeping

110   both Eppendorf micro-centrifuge tubes stationary for two hours. The results did not show

111   any of significant difference in absorbance intensity ($\approx$0.6). Hence, this experiment

112   indicated no interaction of produced formazan salt dye with carbon particles.

113

114 **SI-8 IMARIS 3-D reconstruction images from CLSM analysis for qualitative**
115 **analysis of the biofilm morphology.**

116

+0.3 V Ca   **+0.3 V Pa**

+0.6 V Ca   **+0.6 V Pa**

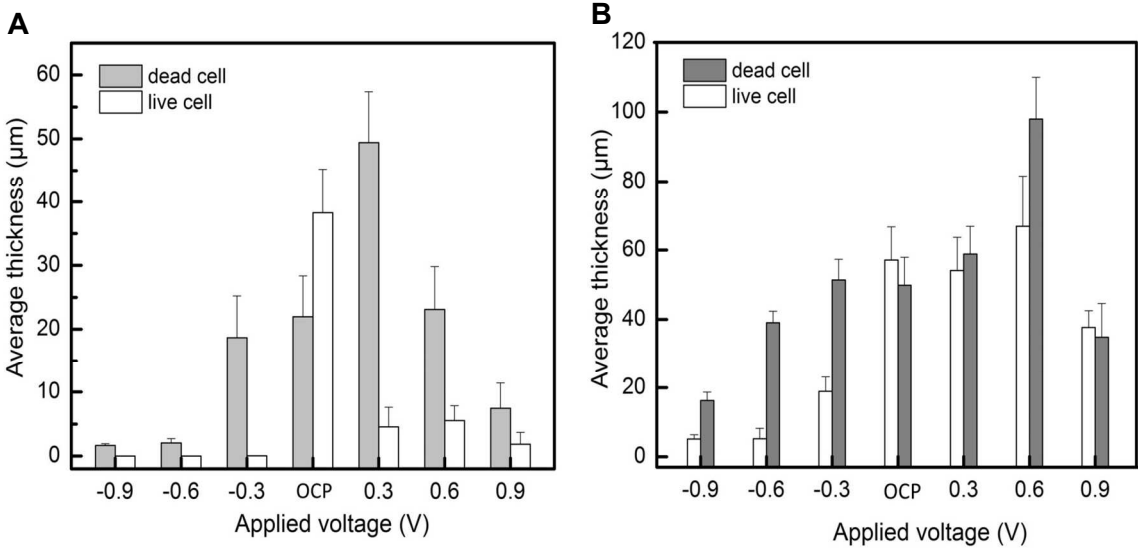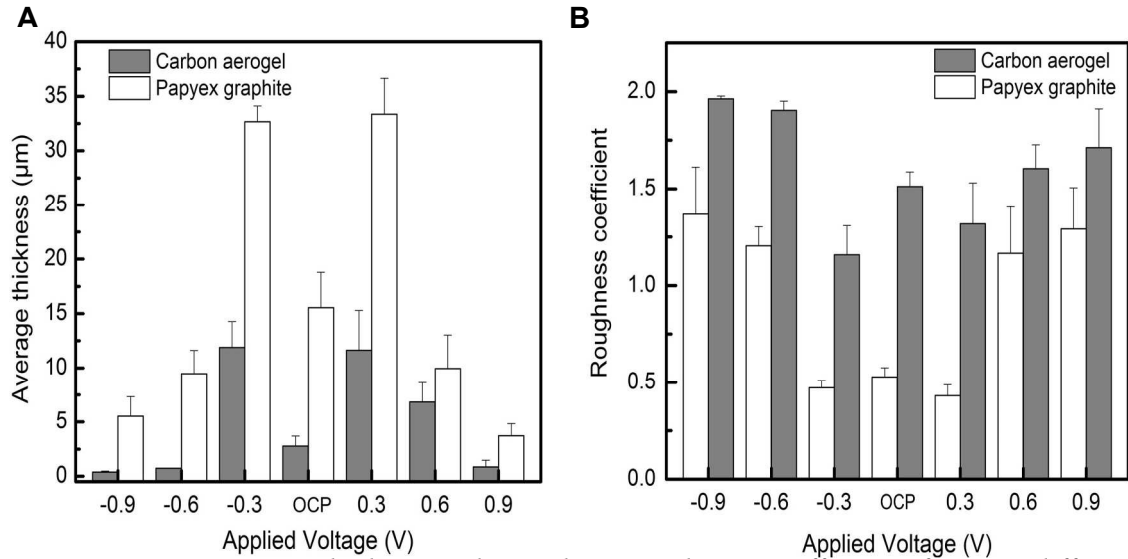**+0.9 V Ca**   **+0.9 V Pa**

117

118   ***Figure S-7:*** *IMARIS 3-D images: The left and right columns present the exemplary*

119   *images from scans of carbon aerogel (Ca) and Papyex graphite (Pa), respectively.*

120   *The red, green, and blue clusters indicate dead cells, live cells, and EPS on electrode,*

121   *respectively. The orange and violet colour indicate overlapping zones of live and*

122   *dead cells, as well as dead cells and EPS, respectively. Figures are perspective*

123   *images 600 μm × 600 μm in size.*

124

125

126 **SI-9 Effect of an electric field on the thickness of biofilm on carbon electrodes**
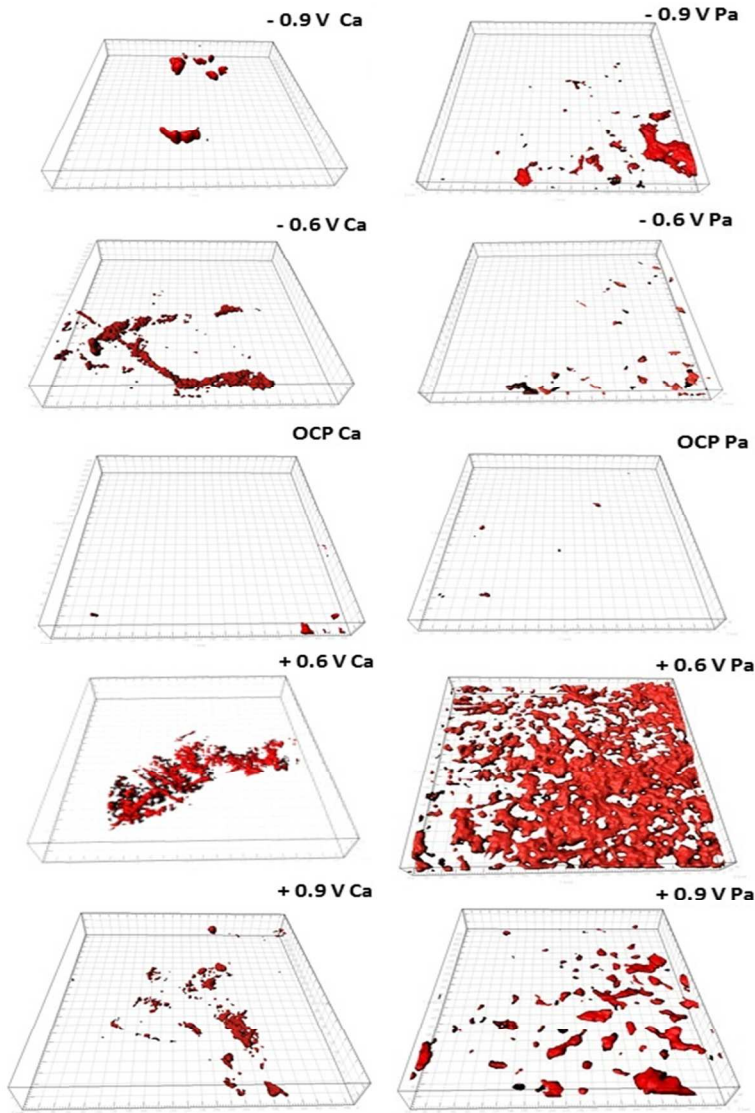
127

128

135

136

137 ***Figure S-8****: The average thickness value at A: CA and B: PA in flow cell experiment*
138 *using 10% LB (Luria-Bertani) medium after 36 hours. Each error bar represents one*
139 *standard error.*

140

141

142   **SI-10 Effect of an electric field on EPS formation on a carbon electrode**

143

144

152   ***Figure S-9****: A: Average thickness value and B: Roughness coefficient of EPS at different*

153   *carbon electrode in flow cell experiment using 10% LB (Luria-Bertani) medium; each*

154   *error bar represents one standard error. 0 V implied open circuit condition (without any*

155   *external applied potential).*

156

157

SI-11 Analysis of intracellular ROS using DHR assay and observed in IMARIS

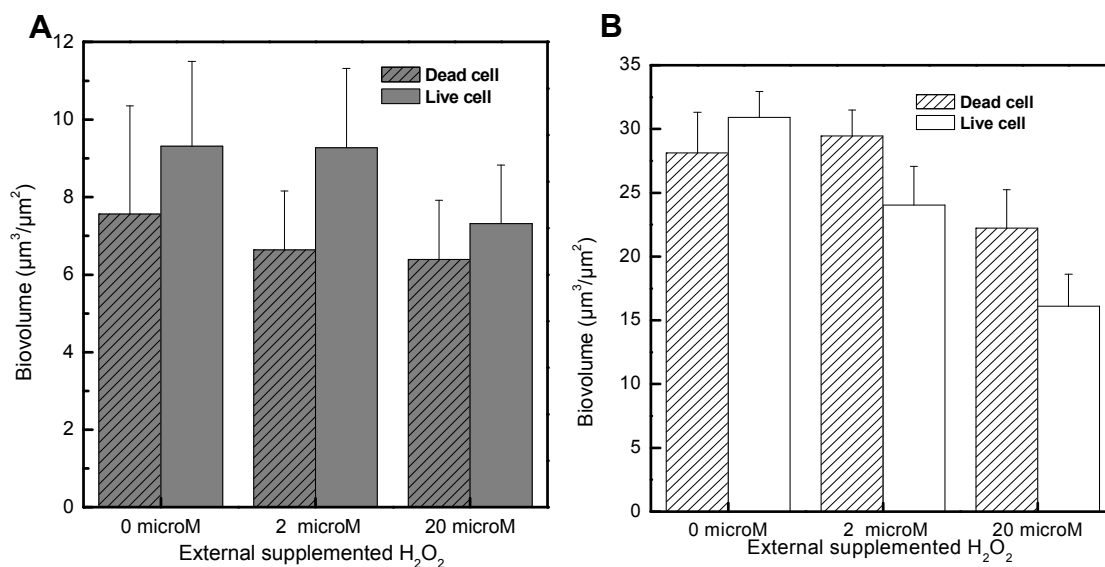**visualizations of the CLSM results**

Figure S-10: *IMARIS 3-D images: Analysis of intracellular ROS using DHR assay. The*

left and right columns present the exemplary images from scans of carbon aerogel (CA)

and Papyex graphite (PA), respectively, polarized at different magnitude of applied

potential. The red cluster indicated DHR stained bacterial cell on electrode. Figures are
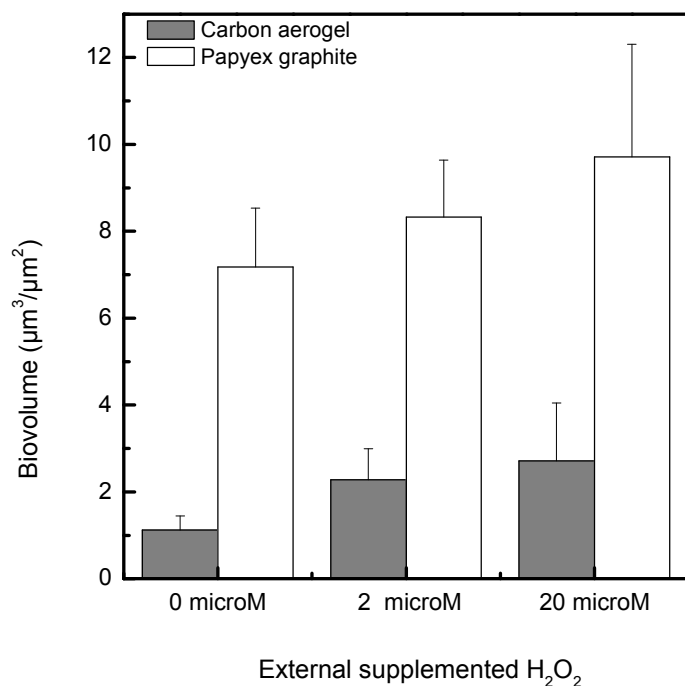
perspective images 600 μm × 600 μm in size.

SI-12 Effect of external dosage of hydrogen peroxide on biofilm formation at OCP condition

In order to provide a quantitative measure for the effect of peroxide on biofilm formation in this study, additional experiments were carried out to confirm the influence of external dosage of HP on biofilm formation at open circuit mode as it is described in this section.

Two different concentrations were supplemented to the flow cell during generation of biofilm on the carbon electrode: 2µM and 20 µM HP (a 10 fold higher in order to evaluate the effect of external HP dosing) at open circuit mode. The effect of external HP dosing at open circuit mode was carried out by providing diluted HP from external source. The generated biomass was now compared with biomass generated without H_2O_2 dosing at OCP. The biovolume generated without HP and with 2µM was almost similar while using 20 µM HP (Figure S-11 A & B), the biovolume for both dead and live cell was slightly lower. This might be due to damage of seed bacteria adsorb on the electrode surface. Similar trend was noticed for both Papyex graphite and carbon aerogel. EPS production increased with increasing dosing of HP suggesting retaliation of biofilm to negate the harmful effect of HP (Figure S-12). This part of the study indicated insignificant effect of HP on biofilm formation when its concentration is lower, which may relate to diffusion limitation in the flow cell. While this experiment was carried out intending to simulate the situation on the electrode under the influence of external electric field, this situation is different from the HP generation on the polarized electrode. At cathodically polarized condition, HP instantly generated on the surface of electrode (Eapp > 0.5 V) and it may cause impairment of bacterial cell adsorbed on the surface of the working electrode due to the intimate proximity of the bacterial cell and the source of HP.

192

Figure S-11: *Biovolumes of dead cell and live cell generated on different carbon*

electrodes after 36 hour of flow cell experiment using 10% LB (Luria-Bertani) medium.

A: CA and B: PA; Each error bar represents one standard error. The X axis represents

different concentration of H_2O_2 supplemented in flow cell.

197

198

Figure S-12: Biovolumes of EPS generated on different carbon electrodes after 36 hour of flow cell experiment using 10% LB (Luria-Bertani) medium. Each error bar represents one standard error. The X axis represents different concentration of H_2O_2 supplemented in flow cell.
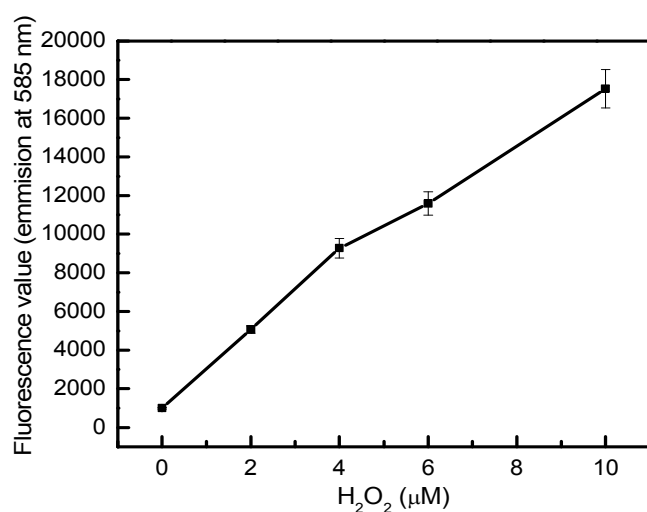
SI-13 Effect of electric field on production of hydrogen peroxide

In order to confirm the generation of HP, under the studied conditions, the Amplex red HP assay was used. A Standard curve for HP quantification using Amplex red® HP assay was provided in S-13. It should be mentioned that the online measurement of HP generation in a continuous flow cell containing bacteria is challenging, because solution collected from the outlet for HP measurement needed filtration to separate detached cells or unwanted clump. In order to resolve these challenges and collecting more accurate data of the electrochemical HP generation, electrodes were polarized without bacterial inoculation while flow cell was kept in batch mode. The batch mode was opted to avoid the possible 'washout' of HP in continuous mode flow cell experiment. This method's

214   implementation could avoid the complication associated with biological matter during the
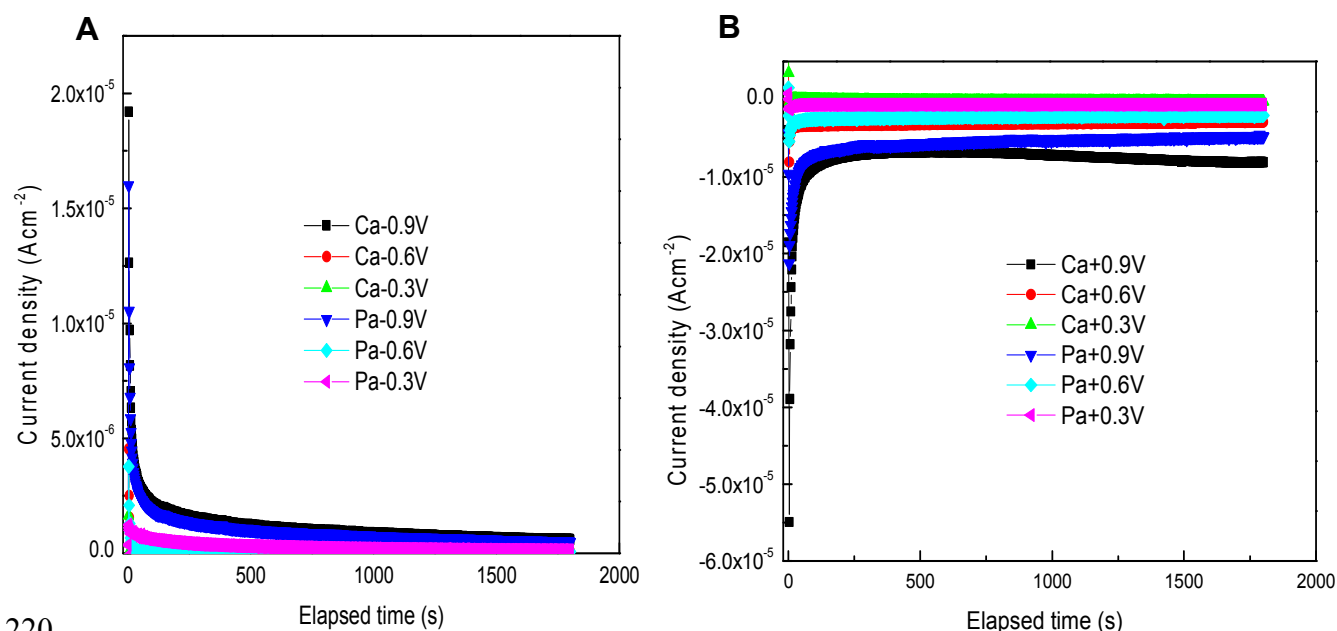
215   HP measurements.

216

217

218

219   ***Figure S-13*** *Standard curve for HP quantification using Amplex red® HP assay*

220

221 ***Figure S-14****: Chronoamperometric profile of both carbon aerogel and Papyex at*
222 *cathodically (A) and anodically (B) polarized condition at the flow cell.*
223

224 The current density recorded during chronoamperometry can be correlated to H_2O_2
225 production at different applied voltages. The current density in the very low range of
226 0.002-0.0001 mA/cm^2 suggested inadequate H_2O_2 generation under the influence of
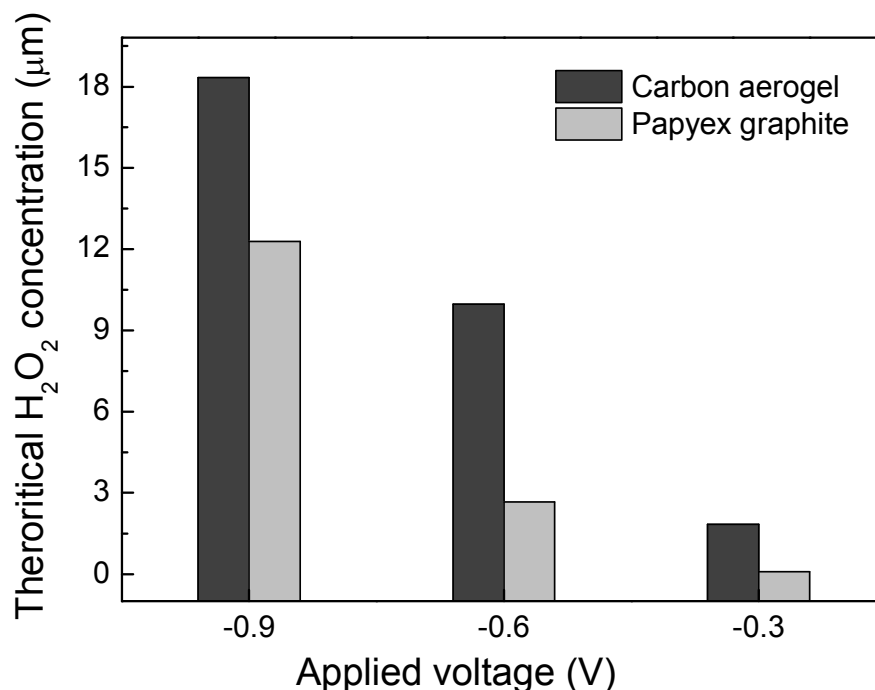227 different magnitude of applied potential (Figure S-14).

228 **Theoretical generation of hydrogen peroxide along the electrode surface.**

229 We estimated the maximum amount of electrochemically generated HP, along the

230 electrode surface based on the current generated at different magnitudes of applied

231 voltage. The maximum theoretical HP concentration was calculated using equation SI-1

232 assuming 100% Faradic current efficiency (CE) utilized for HP generation and constant

233 current during chronoamperometry.

234 $$C_{H_2O_2} = \frac{CE \int i\,dt}{nFV100}$$ Eq. SI-1

235 where $C_{H_2O_2}$ represents H_2O_2 concentration along the electrode surface (in M) and V is the

236 volume of the electrolyte solution inside the flow cell (in L). n is the number of electrons

237 involved in oxygen reduction reaction to H_2O_2 (2) and F is Faraday constant (96500 C

238 mol^{-1} e-) (Peralta et al., 2013). Current efficiency (CE) can be defined as the ratio of the

239 electricity consumed by the electrode reaction of interest over the total electricity passed

240 through the circuit (Qiang et al., 2002). The current density values were deduced from the

241 previous experiment of the batch mode HP generation (Figure S-14). Considering 100%

242 faradic efficiency (i.e., all the electrons are assumed to be utilized for H_2O_2 production),

243   the current density and H_2O_2 production on the two different carbon electrodes iare

244   provided in Figure S-15.

245

246   *Figure S-15: The theoretical concentration of H₂O₂ (µM) generated on CA and PA*

247   *carbon electrodes*

248   Assuming 100% Faradic current efficiency, maximum values of 18and 12 µM HP could

249   be generated along the carbon aerogel and Papyex graphite electrodes, respectively

250   (Figure S-15), while using Amplex red HP assay, a maximum of 2.4 µM of HP was

251   detected. The possible reason for obtaining lower HP concentration during Amplex red

252   HP assay may be due to following reasons: i) instant decomposition of HP; ii) the span

253   of the electrochemically generated HP is short due to instantaneous oxidation of the LB
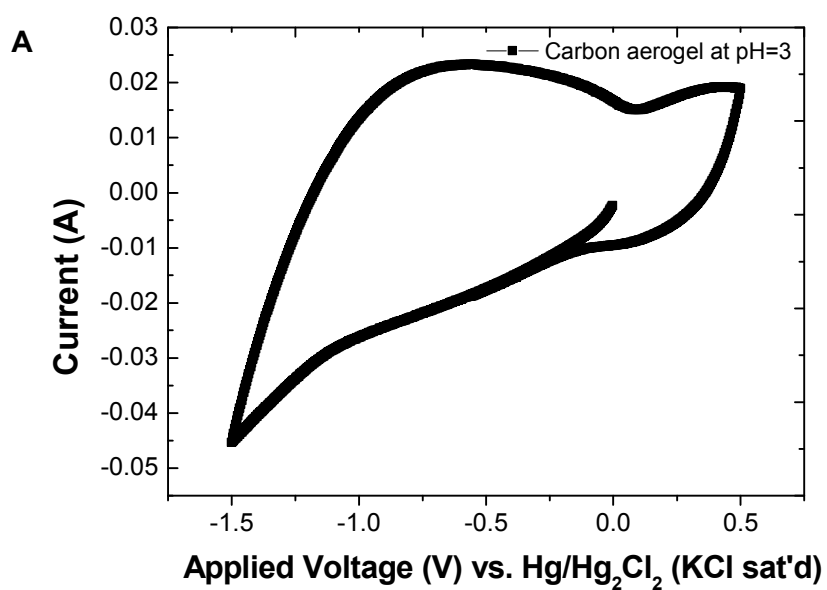
254   medium.

255 In addition, lower concentration of HP may evolve due to physicochemical factors that

256 affect electro- reduction of oxygen. Among them are pH of electrolyte solution, dissolved

257 oxygen concentration and catalytic property of electrode (Sánchez-Sánchez and Bard,

258 2009; Ramaswamy and Mukerjee, 2012).

259 $O_2 + 2H^+ + 2e\text{-} \rightarrow H_2O_2, E^0 = 0.440\,V$ vs. SCE   Eq. SI-2
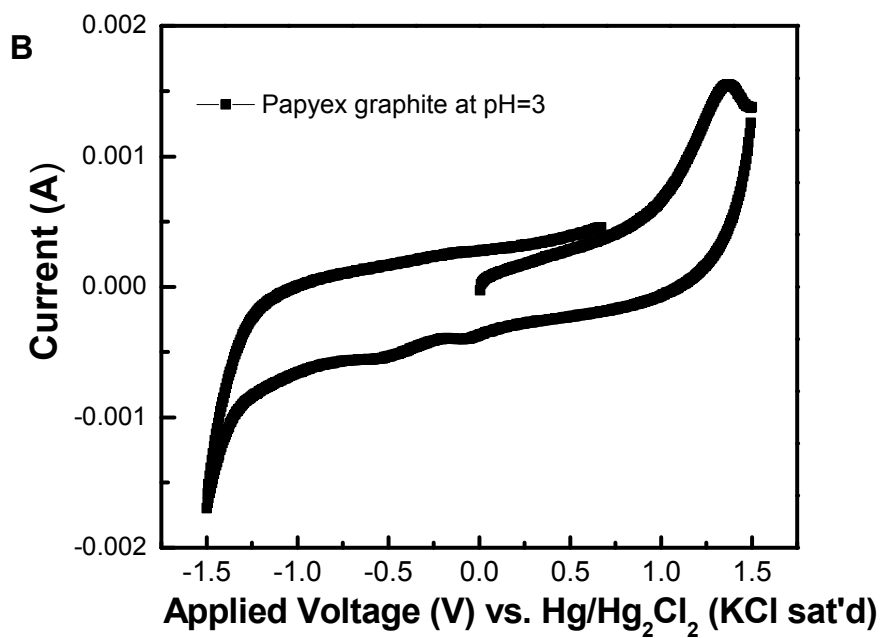
260 It was reported that

261 pH 3 was reported as optimal for the production of hydrogen peroxide (Peralta et al.,

262 2013)). According to Equation SI-2 indicates that high proton concentration favour the

263 production and accumulation of HP. The nearly neutral pH of the LB media in this study

264 was unfavorable for significant amount of HP production.

265 Figure S-16 shows that the electro-catalytic activity of the carbon aerogel and graphite

266 electrodes is poor at neutral pH. No reduction peak for hydrogen peroxide was detected

267 after adjusting the solution to pH 3 (Figure S-16). Probably, this is the reason why

268 researchers used noble metals (according to volcano plot or surface-modified carbon

269 electrodes for electro-reduction of oxygen for efficient HP production (Jiao et al., 2015).

270 Peralta et al. found a distinct peak at -1.0V (vs. Ag/AgCl) for H_2O_2 from O_2 electro-

271 reduction using cyclic voltammetry (Peralta et al., 2013). Whereas, in this study, we

272 didn't observe similar phenomenon.

273

274

275

276 *Figure S-16: Cyclic voltammograms at a scan rate of 5 mV/sec using 0.1 M 0.1 M*

277 *Na2SO4 as an electrolyte at pH 3. A) Working electrodes- Carbon aerogel and B)*

278 *Papyex graphite.*

279 The maximum windows potential range (with respect to saturated calomel electrode) of

280 the present experiment was also not thermodynamically conducive for HP generation

281 (Figure S-2). The maximum cathodic potential with respect to saturated calomel electrode

282 was found around -0.1 to -0.15 mV (Figure S-2). Under this conditions only limited

283 amount of HP generation is expected. Therefore, it can be inferred that all the

284 physicochemical conditions are adverse to HP generation.

285 There are additional reasons, which support the notion that HP effect on the viability of

286 the cells in this study, even at the high calculated magnitude (Figure S-15), is negligible:

287 (i) Catalase (KatA) activity was detected at 50 mM of HP and protected the biofilm cells

288 (Elkins et al., 1999; Stewart et al., 2000) and (ii) relatively high concentration of 44 mM

289 was required to decrease PAO1 biofilm formation (Plyuta et al., 2013).

290 Hence, we conclude that HP generation during the cathodic reduction is sub-inhibitory

291 for biofilm formation. It is noteworthy that bacterial cell viability also reduced when

292 working electrodes were anodically polarized and an elevated intracellular ROS was

293 detected with increase in the magnitude of applied potential. Therefore, the intracellular

294 ROS generation towing to the applied electrode potential is the main cause for the non-

295 viability of the bacterial biofilm cells.

296

297

298   **Reference**s

299   Elkins, J.G., Hassett, D.J., Stewart, P.S., Schweizer, H.P., McDermott, T.R., 1999.
300   Protective role of catalase in Pseudomonas aeruginosa biofilm resistance to hydrogen
301   peroxide. Appl. Environ. Microbiol. 65, 4594–4600.

302   Peralta, E., Natividad, R., Roa, G., Marin, R., Romero, R., Pavon, T., 2013. A
303   comparative study on the electrochemical production of H_2O_2 between BDD and graphite
304   cathodes. Sustain. Environ. Res. 23, 259–266.

305   Pliuta, V.A., Andreenko, I.V., Kuznetsov, A.E., Khmel', I.A., 2013. [Formation of the
306   Pseudomonas aeruginosa PAO1 biofilms in the presence of hydrogen peroxide; the effect
307   of the AiiA gene]. Mol. Genet. Mikrobiol. Virusol. 10–14.

308   Qiang, Z., Chang, J.-H., Huang, C.-P., 2002. Electrochemical generation of hydrogen
309   peroxide from dissolved oxygen in acidic solutions. Water Res. 36, 85–94.
310   doi:10.1016/S0043-1354(01)00235-4

311   Stewart, P.S., Roe, F., Rayner, J., Elkins, J.G., Lewandowski, Z., Ochsner, U.A., Hassett,
312   D.J., 2000. Effect of Catalase on Hydrogen Peroxide Penetration into Pseudomonas
313   aeruginosa Biofilms. Appl. Environ. Microbiol. 66, 836–838.

314   Jiao, Y., Zheng, Y., Jaroniec, M., Qiao, S.Z., 2015. Design of electrocatalysts for oxygen-
315   and hydrogen-involving energy conversion reactions. Chem. Soc. Rev. 44, 2060–2086.
316   doi:10.1039/c4cs00470a

317   Ramaswamy, N., Mukerjee, S., 2012. Fundamental Mechanistic Understanding of
318   Electrocatalysis of Oxygen Reduction on Pt and Non-Pt Surfaces: Acid versus Alkaline
319   Media [WWW Document]. Adv. Phys. Chem. doi:10.1155/2012/491604

320   Sánchez-Sánchez, C.M., Bard, A.J., 2009. Hydrogen Peroxide Production in the Oxygen
321   Reduction Reaction at Different Electrocatalysts as Quantified by Scanning
322   Electrochemical Microscopy. Anal. Chem. 81, 8094–8100. doi:10.1021/ac901291v

323

324